Analysis of Non-volatile Component Differences and Metabolic Pathways in Various Forms of Dracaena cochinchinensis Resin-Containing drugs Using Untargeted Metabolomics and Molecular Networking

Meijia Chen
Heilongjiang University of Chinese Medicine
Yunfei Cui
Yunnan Branch, Institute of Medicinal Plant Development, Chinese Academy of Medical Sciences Peking Union Medical College
Jinhua Su
Xishuangbanna Institute for Drug Contorl
Jiahui Ren
Traditional Chinese Medicine Hospital of Ya'an
Yu zhu
Yunnan Branch, Institute of Medicinal Plant Development, Chinese Academy of Medical Sciences Peking Union Medical College
Jinhui Wang
Xishuangbanna Dai Medicine Research Institute Co ., Ltd
Guang Li
lhbg311@hotmail.com

Yunnan Branch, Institute of Medicinal Plant Development, Chinese Academy of Medical Sciences Peking Union Medical College

Article

Keywords: Resin-Containing drugs in Dracaena, UPLC-Q-TOF-MS/MS, FBMN, multivariate statistical analysis, stress response

Posted Date: July 30th, 2025

DOI: https://doi.org/10.21203/rs.3.rs-7120702/v1

Additional Declarations: No competing interests reported.

Abstract

Objective: The aim of this study is to systematically characterize the non-volatile metabolite profiles of three representative resin-containing drugs—namely, the resin-secreting aggregated sample LZ, the whole body resin-containing sample MZ, and the hollow cork cambium sample P—in Dracaena. By analyzing the patterns of defensive metabolic reprogramming induced by different levels of damage, and elucidating the mechanisms connecting defensive signal transduction with Dracaena Draconis synthesis, we seek to identify theoretical targets for the strategic induction of resin accumulation.

Methods: Three distinct types of morphological samples were systematically analyzed utilizing UPLC-Q-TOF-MS/MS within a non-targeted metabolomics framework. This approach was further enhanced through the construction of FBMN and the application of multivariate statistical analyses, including PCA, PLS-DA, OPLS-DA. Molecular network analysis was conducted using the GNPS platform. Additionally, statistical modeling and differential metabolite screening were executed via MetaboAnalyst and SIMCA, employing criteria of VIP > 1, |FC| > 2, and P < 0.05. Furthermore, KEGG metabolic pathway enrichment analysis was performed to elucidate the biological implications of the identified metabolites.

Results: This study identified 314 non-volatile compounds, primarily flavonoids, lipids, and phenolic derivatives. The OPLS-DA model highlighted significant differences in metabolites among LZ vs. MZ, MZ vs. P, and LZ vs. P groups, with 81, 80, and 30 metabolites, respectively. These were mainly linked to flavonoid biosynthesis, galactose, linoleic acid, and phenylalanine metabolism. The LZ form overexpresses defensive flavonoids, terpenoids, and phenylamines for acute stress response. The MZ form is rich in steroids and fatty acids to maintain lipid balance during chronic drought. The P form enhances lignin monomers for physical barrier repair. These resin-containing medicinal materials from Dracaena cochinchinensis represent a metabolic continuum: P (basic repair), MZ (resin adaptation), and LZ (defensive burst).

1. Introduction

Dracaena Draconis is the main substitute for the traditional Chinese medicine 'Draconis Sanguis, which comes from the red resin of Dracaena cochinchinensis. Used for over 1,500 years in traditional Chinese medicine, it aids blood circulation, stops bleeding, and promotes tissue regeneration[1,2], Modern research indicates that its components, including flavonoids and phenolic acids, have various pharmacological benefits, such as anti-inflammatory, anti-atherosclerotic, anti-tumor, and wound healing properties[3–6].

Dracaena cochinchinensis faces scarcity due to its slow growth and limited habitat, worsened by rising demand and overexploitation. Global warming and environmental damage have further reduced its suitable rainforest areas and wild populations, threatening its future. To address this crisis, researchers are focusing on understanding its resin formation and exploring alternative production methods.Current research suggests that the production of Dracaena draconis is intricately linked to the plant's defense mechanisms. Upon experiencing external mechanical damage or insect predation, Dracaena

cochinchinensis becomes susceptible to infection by pathogenic microorganisms, including Fusarium graminearum and Fusarium moniliforme[7]. These pathogens invade the thin-walled cells of the xylem, thereby activating the plant's secondary metabolic defense system.Flavonoids, terpenoids, phenolic compounds, and other phytochemicals accumulate to form red polymers, which subsequently deposit in stratified layers at the wound site, leading to the formation of Dracaena Draconis. However, Dracaena draco demonstrates distinct defensive mechanisms in response to varying levels of damage, resulting in variations in the resin content of resin-containing pharmacological products derived from different forms of Dracaena. Preliminary investigations have been undertaken to analyze the volatile constituents of resin-containing wood across various forms of resin-based medicinal products in Dracaena. The findings indicate that the metabolites derived from fiber-rich and hollow cork cambium samples (P) exhibit similarities, while those from whole body resin-containing samples (MZ) and resin-secreting aggregated samples (LZ) demonstrate significant differences[8]. Furthermore, the volatile metabolites of resin-containing wood from various forms of Dracaena cochinchinensis also show variability. Consequently, it can be reasonably inferred that there are distinctions in the non-volatile metabolites of resin-containing substances derived from different forms of Dracaena cochinchinensis.Given that the non-volatile constituents of Dracaena draconis play a crucial role in the defense mechanisms and pharmacological properties of Dracaena cochinchinensis, it is proposed that Dracaena draconis employs unique resin synthesis pathways when subjected to diverse stressors. Nevertheless, limited research has established a link between the defense transition response of Dracaena cochinchinensis and its resin synthesis mechanisms. Moreover, the development of artificial lipid synthesis strategies remains constrained due to an insufficient understanding of the interplay between defense mechanisms and lipid synthesis.

Secondary metabolites synthesized by plants are integral to their defense mechanisms and serve as crucial sources of natural pharmaceuticals. Investigating the diversity of these metabolites constitutes a fundamental objective within contemporary life sciences. Metabolomics technology facilitates the systematic examination of the composition and dynamic fluctuations of metabolite pools within organisms, thereby uncovering substantial variations in metabolite structure and abundance across different species, tissues, developmental stages, and environmental conditions. This approach yields valuable insights into the adaptive strategies and health-promoting properties of plants. Currently, researchers predominantly employ a range of separation and detection methodologies, including gas chromatography-mass spectrometry (GC-MS), liquid chromatography-mass spectrometry (LC-MS), ion mobility mass spectrometry (IMMS), and nuclear magnetic resonance (NMR)[9,10], to identify plant constituents. Among these techniques, ultra-performance liquid chromatography-quadrupole-time-of-flight tandem mass spectrometry (UPLC-Q-TOF-MS/MS) is distinguished by its high throughput, ultra-high sensitivity, and robust separation capabilities. Consequently, it is the preferred technology for detecting non-volatile small molecule metabolites in complex biological matrices and for preliminary component identification[11].Nevertheless, a significant challenge in plant metabolite analysis lies in the accurate identification of components. Traditional identification methods are heavily reliant on the manual comparison of experimental mass spectrometry data, such as relative molecular mass and

secondary mass spectrometry fragments, with established databases (e.g., NIST, MassBank, and PubChem) and compounds documented in the relevant literature.

While this approach is effective for identifying known compounds, it is labor-intensive and time-consuming, posing challenges for the identification of novel or rare metabolites not present in spectral databases. Consequently, traditional methods are constrained in their applicability due to the high structural diversity of plant secondary metabolites and the substantial proportion of unknown compounds. To address this limitation, computation-driven annotation strategies are emerging as increasingly vital solutions. The Global Natural Product Social Molecular Networking (GNPS) represents an open mass spectrometry ecosystem that aggregates extensive data from researchers globally. The GNPS cloud computing platform employs a strategy known as Feature-Based Molecular Networking (FBMN)[12], which utilizes a cosine similarity algorithm to cluster compounds with analogous mass spectrometry behavior into molecular families. This is achieved by integrating three-dimensional data encompassing accurate mass-to-charge ratio, retention time, and MS^2 fragment spectrum. Even in instances where the target metabolite lacks a corresponding entry in the database, it is possible to manually deduce the skeleton or functional group of the unidentified compound by examining its proximity within the network and applying the established rules of the cluster. Subsequently, a visual network can be constructed to substantially enhance the identification of unknown metabolites. The integration of metabolomics with Feature-Based Molecular Networking (FBMN) analysis has been extensively employed to investigate variations in metabolites within traditional Chinese medicine and food sources[13,14].

In this study, the focus was on non-volatile secondary metabolites in Dracaena draconis, specifically selecting three types of resin-containing drugs from Dracaena (P, MZ, and LZ) that exhibit markedly different metabolic profiles. The innovative methodology involved the application of UPLC-Q-TOF-MS/MS technology for the analysis of medicinal materials. Additionally, the study employed non-targeted metabolomics in combination with FBMN to facilitate a more comprehensive identification of the constituents present in resin-containing drugs derived from Dracaena cochinchinensis specimens with diverse morphologies. By integrating spatial metabolism patterns with an analysis of defensive phenotype correlations, we have elucidated the mechanisms of metabolic reprogramming involved in the production of Dracaena Draconis resin under varying stress gradients. This study offers theoretical targets for the sustainable production of this resource[8]. The research workflow is illustrated in Fig. 1.

2. Materials and Methods

2.1 Instrument, Medicines and reagents

X500B ultra high efficiency liquid chromatography-quadrupole time-of-flight high resolution mass spectrometry (UPLC-Q-TOF-MS/MS) (ABSCIEX, USA), SB-1200 ultrasonic cleaner (Ningbo Scientz Biotechnology Co., Ltd.), DV215CD 1/100,000 electronic analytical balance (American OHAUS Company), FW80 high speed universal crusher (Tianjin Taiste Instrument Co., Ltd.), ULTRAPURE type pure water

instrument (ELGA LabWater, UK), Sigmal-14 benchtop low-speed centrifuge (Branch Xingyu Technology Development Co., Ltd.). Methylalcohol□Acetonitrile(Thermo Scientific); Other reagents are of analytical reagent. Resin-Containing drugs in Dracaena cochinchinensis are divided into three types according to their morphology: hollow cork cambium sample (P), whole body resin-containing sample (MZ), and resin-secreting aggregated sample (LZ). All samples were provided by Xishuangbanna Jianlong Pharmaceutical Co., Ltd. The samples were consistent with the research conducted by the research team in the early stage, and the loureirin B content in the samples met the pharmacopoeia standards[10].The list is shown in Table 1.

Table 1
Sample information of Resin-Containing drugs in Dracaena from different appearance

NO.	Batch	Source	Morphotype	NO.	Batch	Source	Morphotype
1	200513	Northern Myanmar	P	18	230128	Central Myanmar	MZ
2	200513	Northern Myanmar	P	19	230128	Central Myanmar	MZ
3	200513	Northern Myanmar	P	20	230128	Central Myanmar	MZ
4	200513	Northern Myanmar	P	21	230128	Central Myanmar	MZ
5	200513	Northern Myanmar	P	22	200513	Laos	LZ
6	200513	Northern Myanmar	P	23	200513	Laos	LZ
7	200513	Northern Myanmar	P	24	200513	Laos	LZ
8	200513	Northern Myanmar	P	25	200513	Laos	LZ
9	200513	Northern Myanmar	P	26	200513	Laos	LZ
10	200513	Northern Myanmar	P	27	230128	Laos	LZ
11	200513	Northern Myanmar	P	28	230128	Laos	LZ
12	200513	Central Myanmar	MZ	29	230128	Laos	LZ
13	200513	Central Myanmar	MZ	30	230128	Laos	LZ
14	200513	Central Myanmar	MZ	31	230128	Laos	LZ
15	230128	Central Myanmar	MZ	32	230128	Laos	LZ
16	230128	Central Myanmar	MZ	33	230128	Laos	LZ
17	230128	Central Myanmar	MZ				

2.2 Methods

2.2.1 Solution preparation

The procedure for the synthesis of Resin-Containing drugs in Dracaena cochinchinensis involves the crushing of the drugs, followed by sieving through a No. 3 sieve. The resulting powder is then precisely weighed, with a precise measurement of 2 g being recorded. This powder is subsequently placed into a 100 mL conical flask, to which 50 mL of 95% ethanol is added. The flask is then subjected to ultrasonic cleaning for a duration of 30 minutes. Following this, the flask is subjected to centrifugation at a speed of 10,000 rpm for a duration of 10 minutes. The resultant liquid is then filtered through a 0.22 μm membrane, and the filtrate is added to the sample bottle for subsequent testing. The bottle is then set aside for future use.

2.2.2 HPLC conditions

Using an Acquity UPLC BEHC18 column (150 mm × 2.1 mm, 1.7 μm), the mobile phase was a 0.1% formic acid aqueous solution (A) - acetonitrile (B) gradient elution: 0–2 min, 95% A; 2–3 min, 95–60% A; 3–7 min, 60–40% A; 7–10 min, 40–20% A; 10–13 min, 20%–0 A; 13–15 min, 0–95% A; 16–20 min, 95% A. Column temperature: 40°C; injection volume: 2 μL; flow rate: 0.3 mL/min.

2.2.3 MS conditions

An electrospray ion source (ESI) with positive and negative ion detection modes was used. The scanning ranges of the primary and secondary mass spectra were 100–1,200 m/z and 50–1,200 m/z, respectively. The ionisation voltage (ISVF) was + 5500/-5500 V; the ion source temperature (TEM) was 550°C; and the spray gas (GS1) and auxiliary heated gas (GS2) pressures were 60 psi. The cone hole voltage (DP) was 100 V; the collision energy (CE) was 40 V; the collision energy superposition (CES) was 20 V; and the air curtain gas pressure (CUR) was 35 psi. The data acquisition time was 20 minutes. Nitrogen was used in each gas path.

2.2.4 FBMN construction

The raw mass spectrometry data was converted to the .mzML format using MSConvert software (ProteoWizard toolkit) and imported into MZmine 4.4.3 software for chromatographic peak detection, deconvolution, alignment, and compound feature extraction. The feature list processed by MZmine (including retention time, m/z, and intensity information) and the corresponding MS/MS spectra were exported and uploaded to the GNPS platform for FBMN analysis.The precursor ion mass tolerance and MS/MS fragment ion mass tolerance are both set to 0.02 Da. In order for a comparison to be considered valid, it is a prerequisite that there is evidence of at least six mass-similar fragments, with a similarity score that exceeds 0.7. Spectra should be searched for within the network in public spectral databases (including MassBank, ReSpect, NIST, and other databases).The positive ion mode dataset generated by FBMN can be accessed via the following link: https://gnps.ucsd.edu/ProteoSAFe/status.jsp?task=7e7c68584bdc4f9ba64786aa65d9a2b4; The negative ion mode dataset can be accessed via the following link: https://gnps.ucsd.edu/ProteoSAFe/status.jsp?task=71a7007093c74a58972b82d45ed1761e. Visualise the created network using Cytoscape 3.10.1.

2.2.5 Multivariate statistical analysis

MetaboAnalyst 6.0 was used to perform PCA and PLS-DA on the data matrix obtained from FBMN analysis (all metabolite features and their intensities in all samples) to observe the overall distribution of the samples. OPLS-DA was performed using SIMCA 14.0. Important metabolites were identified based on variables that met the criteria of VIP > 1, P < 0.05, and |FC| >2. KEGG pathway enrichment analysis was performed on the differentially expressed metabolites in each group, and the threshold value for the metabolic pathway influence value was set to 0. Values above this threshold were selected as potential target pathways.

3. Results

3.1 UPLC-Q-TOF-MS/MS analysis of three forms of Dracaena Draconis

To investigate the compositional variations among different morphological types of Resin-Containing drugs in Dracaena, a non-targeted UPLC-Q-TOF-MS/MS analysis was conducted on three distinct morphological samples: the hollow cork cambium sample (P), the whole body resin-containing sample (MZ), and the resin-secreting aggregated sample (LZ). A comprehensive analysis was performed on all samples in both positive and negative ion modes, resulting in the generation of total ion current spectra for LZ, MZ, and P, as depicted in Figure S1. As illustrated in Figure S1, there are observable differences in the number and intensity of the peak groups across the samples, indicating significant variations in the types and concentrations of metabolites present in the resin-containing drugs of Dracaena cochinchinensis across these three morphological types.

3.2 Exploring the chemical space characteristics of three morphological groups of Dracaena Draconis through FBMN

This study utilized Feature-Based Molecular Networking (FBMN) technology to analyze the chemical compositions of various Dracaena draconis samples. In the positive ion mode, 44,008 metabolite features were detected, resulting in the formation of 12,757 molecular families (defined as having ≥ 2 nodes) through FBMN analysis, as depicted in Figure S1. In the negative ion mode, 23,040 metabolite features were identified, leading to the recognition of 5,774 molecular families (each with ≥ 2 nodes). The nodes are visually represented by color-coded pie charts, indicating the relative abundance of metabolites across three groups: red for MZ, green for LZ, and blue for P, as shown in Figure S2. Notably, larger nodes correspond to compounds identified within the GNPS database. In total, 238 compounds were identified within the positive ion mode network, and 102 compounds were identified within the negative ion mode network. After deduplication, a cumulative total of 314 unique compounds were identified. The NPClassifier is an advanced tool based on deep neural networks, specifically designed for the automatic classification of natural products according to their structural characteristics. This classification is achieved through the application of Morgan Fingerprints[15]. The NPClassifier was

employed to categorize three types of Dracaena draconis metabolites into 16 distinct groups, including flavonoids and their derivatives (81), lipids (65), phenolic derivatives (50), steroids (18), and carbohydrates and glycosides (17). As depicted in Fig. 1, the spectrum of chemical compounds analyzed includes alkaloids and their derivatives (17), terpenoids (17), lignans and novel lignans (16), coumarins (10), peptides (8), polyketides (3), naphthalenes (4), heterocyclic compounds (4), macrolides (2), alcohols and polyols (1), and nucleosides (1). It is evident that among the metabolites of Dracaena draconis, flavonoids, lipids, and phenolic compounds hold primary significance. The numbers in parentheses indicate the quantity of compounds within each category, as shown in Figure S4.

3.3 Structure analysis and pharmacological action of metabolites

The FBMN algorithm has been shown to aid in the clustering of compounds with similar MS2 fragmentation patterns into molecular families. An in-depth manual analysis of compound structures was performed to investigate the structural interconnections among components within the flavonoid, lipid, phenolic acid, and terpenoid molecular families. Subsequently, the chemical structural relationships within these molecular groups were visually depicted.

3.3.1 Annotations of flavonoid molecular families

Flavonoids represent the primary chemical constituents of Dracaena draconis and exhibit significant pharmacological activity. The structural diversity of these compounds has been shown to directly influence the quality of medicinal materials. This study focused on the flavonoid molecule family (Fig. 2) in alignment with the FBMN molecular network clustering results. High-resolution mass spectrometry fragmentation analysis was utilized, alongside characteristic fragment ions and neutral loss patterns, to systematically elucidate the fragmentation pathways and structural characteristics of five key flavonoid compounds. This methodology provides a foundational basis for interpreting the functional implications of metabolic differences.This methodology establishes a foundational framework for the functional interpretation of metabolic variations. Flavonoid compounds possess a core C15 benzopyranone structure, which is further categorized into various subclasses based on the substituents present on the A and B rings, the saturation level of the C ring, and the sites of glycosylation. The predominant cleavage mechanism is Retro-Diels-Alder (RDA) cleavage, which generates characteristic fragments from the A/B rings (e.g., m/z 137, 129). In the positive ion mode, protonation sites are preferentially situated at the carbonyl or hydroxyl groups of the C ring, resulting in major fragments such as decarboxylation (-44 Da), decarbonylation (-28 Da), and dehydration (-18 Da) products[16–18].

The MS1 analysis of compound A reveals a precursor ion at m/z 255.1 $[M + H]^+$, suggesting a molecular formula of $C_{15}H_{10}O_4^+$. The fragmentation pathway, depicted in Fig. 3A, demonstrates that in positive ion mode, $C_{15}H_{10}O_4$ undergoes RDA fragmentation, yielding $C_7H_5O_3^+$ (m/z 137), which subsequently undergoes secondary carbon monoxide (CO) loss to form $C_6H_5O_2^+$ (m/z 109). Additionally, the CO loss

from $C_{15}H_{10}O_4^+$ results in the formation of $C_{14}H_{10}O_3^+$ (m/z 227). Based on these fragmentation patterns and corroborated by databases such as HMDB, ChEBI, DrugBank, and PubChem, compound A is identified as 4,7-dihydroxyflavone.

The molecular ion of compound B was observed at m/z 241.1 $[M + H]^+$, suggesting a molecular formula of $C_{15}H_{12}O_3^+$. The fragmentation pathway of this ion is illustrated in Fig. 3B. The molecular ion undergoes RDA fragmentation, leading to the cleavage of the 7-hydroxymethyl group ($C_7H_5O_3^+$) at m/z 137.0. Subsequently, the ion at m/z 137.0 undergoes further fragmentation with the loss of carbon dioxide (28 Da), resulting in the formation of a phenyl ketone ion ($C_6H_5O_2^+$, m/z 109.0). Based on these fragmentation pathways, and corroborated by data from HMDB, KNApSAcK, ChEBI, DrugBank, and other pertinent literature sources[19,20], it is hypothesized that the compound is 7-hydroxyflavanone.

The MS1 of compound C reveals its precursor ion at m/z 239.1 $[M + H]^+$, with the proposed molecular formula $C_{15}H_{10}O_3^+$. The fragmentation pathway is depicted in Fig. 3C: initially, the 7-hydroxy group attacks the carbonyl group, leading to cleavage of the C ring and the formation of an indanone structure, resulting in $C_9H_5O^+$ (m/z 129). Subsequently, ring cleavage occurs, accompanied by decarboxylation or hydrogen transfer, yielding $C_7H_5O_3^+$ (m/z 137). The B ring is further cleaved to produce the benzyl ion $C_6H_5^+$ (m/z 77). Based on these fragmentation pathways, along with corroborative data from databases such as MassBank, HMDB, COCONUT, and existing literature[21], the compound is tentatively identified as 7-hydroxyflavone.

The MS1 analysis of compound D reveals its precursor ion at m/z 257.1 $[M + H]^+$, corresponding to the proposed molecular formula $C_{15}H_{12}O_4^+$. The fragmentation pathway of this compound is depicted in Fig. 3D. Key stages in this process include the retro-Diels-Alder (RDA) cleavage of the A ring, the cleavage of the dihydrofuranone ring (C ring), and the formation of a stable benzofuranone ion ($C_7H_5O_3^+$) at m/z 137.02, as well as C_8H_7O + at m/z 119.05, originating from the A ring with a 4'-hydroxy substitution. Additionally, a benzyl ketone ion ($C_8H_7O_2^+$) at m/z 147.05 can be formed through the rearrangement of the A ring hydroxyl group. Based on these fragmentation pathways, alongside database references such as HMDB, ChEBI, and DrugBank, as well as literature reports[22,23], it is hypothesized that compound D is isoliquiritigenin.

The MS1 of compound E shows its precursor ion as m/z 287.1[M + H]+, with the proposed molecular formula $C_{16}H_{14}O_5^+$. The mass spectrometry fragmentation pathway is illustrated in Fig. 3E: the B-ring carbonyl rearranges to form $C_8H_7O_4^+$ (m/z 167); the rearrangement of the A ring with the C2-C3 portion yields a benzoate cation derivative ($C_9H_7O_2^+$) (m/z 147). In view of the above fragmentation pathways, in conjunction with the HMDB and PubChem databases, the compound in question is tentatively identified as 4'-5-dihydroxy-7-methoxyflavanone.

The integration of multi-level mass spectrometry fragment data with molecular network clustering has facilitated the identification of key flavonoid metabolites, including 4,7-dihydroxyflavone (A), 7-hydroxyflavanone (B), 7-hydroxyflavone (C), isoliquiritigenin (D), and 4',5-dihydroxy-7-methoxy dihydroflavone (E). These compounds are crucial for Dracaena draconis's stress defense and their distribution supports further metabolic function analysis. Additionally, they exhibit diverse pharmacological effects. For instance, 4,7-dihydroxyflavone can form N-O hydrogen bonds with HIF-1α via THR-327 residues, enhancing anemia[24]. Moreover, 7-hydroxyflavone[25]shows potential in treating protein diseases by binding to Hb near high-affinity amino acid sequences, protecting it from crowding-induced denaturation. Moreover, it has been demonstrated to exhibit cardioprotective and antioxidant properties, suggesting a potential therapeutic advantage in addressing cardiotoxicity induced by the first-line chemotherapy agent doxorubicin[26]. Additionally, 7-Hydroxyflavone has been identified as a promising pharmaceutical candidate for the treatment of osteoporosis. This study hypothesizes that the prevention of dexamethasone-induced osteoporosis is mediated through the modulation of the GATA-3/Caspase-3/NF-KB pathway. Beyond these attributes, the compound displays a range of pharmacological activities, including antioxidant, anti-inflammatory, and vascular protective effects[27–30].As a bioactive compound, isoliquiritinide has demonstrated neuroprotective properties and potential therapeutic benefits for neurodegenerative diseases such as Alzheimer's Disease (AD) and Parkinson's Disease (PD). The principal mechanism underlying the effects of isoliquiritinide is its ability to act as a neuroprotective agent and antioxidant, thereby reducing excessive reactive oxygen species (ROS)-mediated neuronal damage in the brain[31]. To date, 4'-5-dihydroxy-7-methoxyflavone (7-O-methylnaringin) has been documented to exhibit a limited range of pharmacological effects. Nonetheless, research has identified its anti-inflammatory[32]and anti-malarial properties[33], among other effects.

3.3.2 Annotations of the phenolic compound family

The molecular family of phenolic compounds is shown in Fig. 3A.The MS1 of compound A indicates that its quasi-molecule ion is m/z 212.7 $[M + H]^+$, with a fitted molecular formula of $C_{11}H_{14}O_4^+$. The fragmentation pathway of the subject is illustrated in Fig. 3B.The β-cleavage of the propylene alcohol side chain results in the loss of CH_2OH, forming a stable phenylpropyl ion ($C_{10}H_{11}O_3^+$) (m/z 161.1). Subsequent to this, the loss of CO results in the formation of a decarboxylation fragment ($C_9H_{11}O_2^+$) (m/z 133).The initial step in this process is the loss of a carbon monoxide atom, which results in the formation of a phenylpropyl fragment ($C_8H_{11}O^+$) or a benzyl ion ($C_8H_9^+$) (m/z 105.1). This process occurs through the direct cleavage of the benzene ring.In consideration of the aforementioned cleavage pathways, in conjunction with the HMDB, DrugBank, PubChem databases, and reference[34], it is hypothesised that compound A is the lignin monomer sinapyl alcohol.

Sinapic alcohol is acknowledged as a precursor in lignin biosynthesis[35]. The enzymatic conversion of cellulose into lignin compounds within plant cell walls confers mechanical strength and durability to woody tissues. This lignification of cell walls serves as a crucial barrier against pathogen invasion[36]. Beyond its pivotal role in plant physiological processes, sinapic acid exhibits significant potential in

therapeutic applications. Extensive research has demonstrated that mustard oil and its derivatives not only possess anti-inflammatory properties[37] but also mitigate the increase in vascular permeability induced by acetic acid in murine models. Additionally, they inhibit the production of NO, PGE2, and TNF-α triggered by LPS. Moreover, these compounds exhibit notable biological activities, including antioxidant effects, myocardial protection, and the enhancement of skin wound he-aling[35].

3.3.3 Annotation of the molecular family of terpenoids

Terpenoids have been identified as active constituents in Dracaena draco. In the MS2 analysis of terpenoids, several processes are observed, including RDA cleavage, the loss of neutral molecules such as water (H_2O, 18 Da) or carbon monoxide (CO, 28 Da), and the cleavage of saturated rings. The terpenoid molecular family is depicted in Fig. 3C.

The MS1 of compound A reveals a quasi-molecular ion at m/z 205.2 $[M + H]^+$, with a proposed molecular formula of $C_{15}H_{26}O^+$. The fragmentation pathway of this compound, as elucidated through mass spectrometry, is illustrated in Fig. 3D. The cyclohexane ring undergoes RDA cleavage, resulting in the formation of a stable allylic ion ($C_9H_{13}^+$) at m/z 121.1 and a neutral fragment C6H13O following ring cleavage. The allylic ion subsequently undergoes the loss of a vinyl group ($-C_2H_4$), leading to the formation of $C_7H_9^+$ (m/z 93.07) and a neutral fragment C2H4. Based on these cleavage pathways and corroborated by literature reports[38], compound A is hypothesized to be α-bisabolol.

In recent years, α-bisabolol has garnered significant interest within the scientific community. Numerous studies have demonstrated that α-bisabolol possesses the ability to modulate various signaling molecules, including IL-6, IL-1β, IL-17A, IL-23, and TNF-α, thereby exerting anti-inflammatory effects[39–41]. The potential therapeutic applications of α-bisabolol encompass the treatment of conditions such as psoriasis, osteoarthritis, and other related diseases. Furthermore, α-bisabolol has been identified to exhibit anticancer properties[42]through multiple mechanisms, including the downregulation of the AKT signaling pathway, inhibition of vascular endothelial cell proliferation, and induction of apoptosis in tumor cells.

3.4 Multivariate statistical analysis

3.4.1 PCA analysis of Resin-Containing drugs in Dracaena cochinchinensis with different morphologies

A series of multivariate pattern recognition analyses were conducted on the collected and organized data, employing the Principal Component Analysis (PCA) model to investigate the differences in non-volatile metabolites among resin-containing drugs derived from Dracaena cochinchinensis with varying morphologies. As illustrated in Fig. 4A, the coordinate axes PC1 and PC2 denote the two principal components with the highest contribution rates in the PCA. The individual points in the figure represent resin-containing drugs from Dracaena cochinchinensis with distinct morphologies. The PCA model

effectively segregates the samples into three distinct clusters, with the metabolite profiles of the 33 samples in each group exhibiting variations along the PC1 and PC2 axes. The contribution values for PC1 and PC2 are 17.4% and 8.1%, respectively, culminating in a total contribution rate of 25.5%. The overall distribution pattern of the samples indicates that the PCA of the three sample groups shows significant overlap, suggesting that the composition of non-volatile metabolites in resin-containing drugs from Dracaena cochinchinensis with different morphologies exhibits considerable similarity.PCA was insufficient in fully capturing the specific differences between the groups. To enhance the analysis, supervised models such as PLS-DA and OPLS-DA should be utilized in conjunction with the screening of key differential metabolites.

3.4.2 PLS-DA analysis of Resin-Containing drugs in Dracaena cochinchinensis with different morphologies

In order to further distinguish among the various groups, supervised PLS-DA was employed for data analysis. As illustrated in Fig. 4B, the internal aggregation of Resin-Containing drugs in Dracaena cochinchinensis samples of different forms is more pronounced than that observed with the PCA method, exhibiting smaller intra-group and inter-group differences, and each group shows distinct separation along the X-axis. The observed inter-group differences are primarily attributed to the first principal component (PC1), which has a contribution value of 9.7%. However, the overall explanatory power of the PLS-DA model is limited, accounting for only 23.1% of the total variation. This limitation suggests the presence of additional factors influencing inter-group differences. Therefore, further permutation tests should be conducted to analyze these differences comprehensively. In the score plot, the position of MZ between P and LZ indicates its transitional metabolic profile.

3.4.3 OPLS-DA analysis of Resin-Containing drugs in Dracaena cochinchinensis with different morphologies

To further explore the variations in non-volatile metabolites in resin-containing drugs derived from Dracaena cochinchinensis of distinct morphologies, Orthogonal Partial Least Squares Discriminant Analysis (OPLS-DA) models were developed to facilitate comparative analysis between two sample groups, thereby identifying metabolite differences. OPLS-DA, a supervised discriminant analysis statistical technique, was employed in this study using the MetaboAnalyst 6.0 platform and SIMCA 14.0 software to construct OPLS-DA models and conduct permutation test analyses for the LZvsMZ, MZvsP, and LZvsP groups. As illustrated in the score plots (Figs. 4C, E, and G), the sample data for the LZvsMZ, MZvsP, and LZvsP groups are distinctly positioned on opposite sides of the score plots, indicating significant intergroup differences. This suggests that the model is proficient in distinguishing samples from different groups, achieving complete separation, which is conducive to the identification of distinct metabolites. In conclusion, there are discernible differences in the types of non-volatile metabolites present in resin-containing drugs from Dracaena cochinchinensis with varying morphologies.The robustness of the model was further evaluated through additional testing employing a technique known as OPLS-DA replacement testing. As illustrated in the score plots (Figs. 4C, E, and G) and Table S2, the P-

values obtained from the OPLS-DA model replacement testing were all below 0.05, signifying that the differences observed between the groups in the pairwise comparisons were statistically significant. The R2Y and Q2 values of the model indicate that the original model effectively accounts for the differences among the sample groups, with both R2Y and Q2 values approaching 1. Furthermore, the Q2 point regression line intersects the x-axis at a value less than 0, with a negative intercept, suggesting that the statistical model is robust and not subject to overfitting.

3.4.4 Screening of metabolites with significant differences in Resin-Containing drugs in Dracaena cochinchinensis of different morphologies

In this study, VIP values exceeding 1 were employed as the criteria for preliminarily identifying differentially expressed metabolites between groups. Subsequent single-variable statistical analyses were conducted to confirm the significance of these differentially expressed metabolites. Metabolites with VIP values greater than 1, |FC| values exceeding 2, and P-values less than 0.05 were identified as significantly differentially expressed metabolites.

As a total of 81 metabolites exhibited significant differences between the LZ and MZ groups, with 51 metabolites upregulated in the LZ group and 30 in the MZ group. Similarly, 80 significantly different metabolites were identified between the MZ and P groups, with 38 upregulated in the MZ group and 42 in the P group. In the comparison between the LZ and P groups, 30 metabolites showed significant differences, with 11 upregulated in the LZ group and 19 in the P group. The volcano plot analysis for the LZ vs. MZ, MZ vs. P, and LZ vs. P groups is depicted in Fig. 6 (A, B, C). The number of compounds exhibiting differences follows the pattern: LZ vs. MZ ≈ MZ vs. P > LZ vs. P.

Metabolites differing between comparison groups (VIP > 1, |FC| >2, and P < 0.05) were subjected to clustering analysis (Figures S5, S6, and S7). The compounds with the highest content in each group (LZ, MZ, and P) were identified based on peak area (Tables S3, S4, and S5).

Among the 50 differentially expressed metabolites exhibiting elevated expression levels in the LZ sample, 34 were identified using the positive ion mode, while 16 were identified using the negative ion mode. The metabolites identified in this study predominantly comprised phenylamines, flavonoids, and lipid signaling molecules, such as ferulic acid, apigenin, and linoleic acid. Collectively, these metabolites constitute an acute chemical defense network. In the MZ sample, a total of 47 differentially expressed metabolites were identified, with 44 detected in the positive ion mode and 3 in the negative ion mode. The analysis indicated elevated levels of steroids, structural lipids, and long-acting defense compounds, including cholesterol, γ-linolenic acid, and ruscogenin. These findings suggest that the MZ sample sustains active metabolism aimed at maintaining lipid homeostasis. In the P sample, 50 differentially expressed metabolites were detected, with 47 identified in the positive ion mode and 3 in the negative ion mode. The metabolites under investigation were primarily lignin monomers, suberin constituents, and renewable energy compounds, such as pinene, palmitamide, and cotton sugar, which have been

shown to aid in the restoration of physical barriers. Box plots were generated for nine principal differential metabolites, as depicted in Fig. 6(D-L), encompassing α-bisabolol (D), ferulic acid (E), 7-hydroxyflavone (F), linoleic acid (G), γ-linolenic acid (H), cholesterol (I), ruscogenin (J), pinene (K), and cinnamaldehyde (L).

The analysis of the screening results for various metabolites in resin-containing drugs derived from Dracaena cochinchinensis indicates significant spatial heterogeneity in the distribution of metabolites across different forms of Dracaena Draconis.

Resin-secreting aggregated samples (LZ) form sealed storage units within the resin duct chambers, which are more conducive to the storage and secretion of fat-soluble metabolites. Consequently, defensive flavonoids, phenolic acids, and terpenoid compounds predominate.The flavonoid compounds isoliquiritin, apigenin, and 7-hydroxyflavanone have been demonstrated to play a pivotal role in the body's defense against inflammation by inhibiting the NF-κB pathway, while simultaneously enhancing antioxidant activity through the activation of the Nrf2 pathway[43,44]. As a component of essential oils, α-bisabolol, a naturally occurring sesquiterpene, exhibits notable biological activities, including strong anti-inflammatory and antibacterial properties[42]. Phenolic derivatives, functioning as plant antitoxins, are rapidly synthesized at sites of plant injury. They inhibit microbial growth by disrupting cell membranes, thereby eradicating microorganisms such as fungi and bacteria. Additionally, these compounds have the ability to neutralize reactive oxygen species, reduce oxidative damage, and maintain cellular integrity[45,46]. This study investigates the hypothesis that the accumulation of sugar metabolites, such as sucrose and stachyose, can enhance the energy supply in plants, thereby enabling them to better withstand external environmental stress.

Whole body resin-containing samples (MZ) exhibit uniform lipid infiltration within the thin-walled cells of the xylem, devoid of specialized chambers. The substances present are predominantly steroidal saponins and lipid compounds. Cholesterol has been shown to enhance membrane lipid stability and decrease ion leakage. Furthermore, γ-linolenic acid has been demonstrated to regulate genes associated with chronic stress. Additionally, ruscogenin has been identified as being integrated into the plasma membrane, where it forms a hydrophobic barrier. This lipid infiltration phenomenon provides comprehensive protection to entire cells by enhancing membrane stability and reducing transpiration, thereby facilitating adaptation to prolonged drought conditions.

In samples of hollow cork cambium (P), cork cells encapsulate vascular bundles with multiple layers of suberised cells. This configuration facilitates the release and storage of volatile compounds, such as phenylpropanoids, and the deposition of lignin, while also enhancing the long-distance transport of water and nutrients. Consequently, this structural arrangement contributes to both structural defense and mechanical support[47]. Lignin monomers, including pinene and mustard alcohol, are incorporated into the cell walls and subsequently catalyzed by plant-derived peroxidase (POD) to form G/S-type lignin. The synthesis of this lignin type enhances the compressive strength and hydrophobicity of the wood. Additionally, the antioxidant trans-pterostilbene is sequestered within the cork gaps, where it functions

by inhibiting NADPH oxidase, thereby mitigating ROS bursts. This process prioritizes tissue repair and the reconstruction of the physical barrier. Pinene aldehyde, a key aldehyde component in plant lignin, further augments the mechanical strength of plant cell walls by modulating the composition, structure, and chemical properties of lignin polymers, thereby enhancing the efficiency of biomass for sustainable utilization[48,49]. The lignin-suberin complex serves as a mechanical barrier, promoting wound closure, moisture retention, and the regeneration of vascular tissue.

3.4.5 Differential metabolite pathway enrichment analysis

Metabolites exhibiting significant differences between the groups were identified through a series of pairwise comparisons, with the top 25 compounds in each of the three forms (LZ, MZ, and P) being selected based on peak area rankings. Subsequent KEGG pathway enrichment analysis of these compounds yielded three distinct enrichment pathway diagrams (Figs. 7A, 7B, and 7C), which visually represent the biological pathways enriched by the characteristic metabolites of each form.

In the LZ phenotype, differentially expressed compounds exhibited significant enrichment in pathways including linoleic acid metabolism, flavonoid biosynthesis, galactose metabolism, starch and sucrose metabolism, sphingolipid metabolism, and phenylpropanoid biosynthesis. Conversely, in the MZ form, these compounds were enriched predominantly in steroid biosynthesis and phenylpropanoid biosynthesis pathways. The P pattern demonstrated enrichment in starch and sucrose metabolism, α-linolenic acid metabolism, phenylpropanoid biosynthesis, galactose metabolism, and flavonoid biosynthesis. Notably, phenylpropanoid biosynthesis emerged as a common pathway across all three forms. In contrast, sphingolipid metabolism and linoleic acid metabolism were pathways uniquely associated with the LZ phenotype, while steroid biosynthesis was exclusive to the MZ form. Furthermore, α-linolenic acid metabolism was identified as a pathway specific to the P pattern.

Pathway analysis suggests that the synthesis of various lipid forms in Dracaena draconis constitutes a metabolic strategy for plant differentiation in response to environmental stress. This strategy is facilitated by the synergistic effects of JA signal dynamic regulation, competition among branching metabolic pathways, and the remodeling of tissue functions. The central regulatory network of this system is anchored in the phenylpropanoid pathway, with downstream metabolic fluxes diverging based on the intensity and duration of stress, leading to the emergence of three distinct adaptive phenotypes.

The resin-secreting aggregated sample (LZ) functions as an emergency defense mechanism. Linoleic acid serves as a direct precursor in the biosynthesis of JA[50]and is a crucial component of plant cell membranes, energy reserves (such as triacylglycerols), and external barriers (including cutin and suberin). Pathway enrichment analyses indicate that the morphology of LZ is influenced by high-intensity stress. In instances of severe mechanical damage or pathogen infection, linoleic acid is swiftly converted into jasmonic acid, which subsequently promotes the biosynthesis of jasmonic acid-mediated defense responses and orchestrates the plant's stress response[51]. This process rapidly activates key enzymes, including those involved in the phenylpropanoid-flavonoid pathway (such as CHS[52] and FLS),

the phenylpropanoid-phenolic acid pathway (such as HCT[53]), and the isoprenoid pathways (such as TPS[54] and CYP450[55]). In response to stress, plants exhibit short-term adaptive strategies by reallocating resources towards the production of defensive compounds with antibacterial and antioxidant properties, such as flavonoids, phenolic acids, and terpenoids, which consequently inhibit structural growth. Notably, the flavonoid biosynthesis pathway is significantly enriched in LZ, with the core components of the resin accumulating at the site of injury. Flavonoid monomers are effectively polymerized to form Dracaena draco, which acts to seal wounds. This process establishes a chemical barrier that impedes pathogen invasion and exhibits both antioxidant and antibacterial properties[56]. Galactose metabolism facilitates the provision of sugar donors, such as UDP-galactoside, which modify flavonoids to enhance their solubility and transport efficiency. This modification promotes their diffusion within vascular bundles and their subsequent oxidative polymerization into a deep red resin. Consequently, the LZ pattern emerges as a result of the synergistic effects of a surge in jasmonic acid signaling, a burst in flavonoid synthesis, and glycosylation modification under conditions of high-intensity stress, thereby forming a localized lipid-rich structure.

Whole-body resin-containing samples (MZ) are indicative of chronic adaptation in plants. Under conditions of sustained chronic stress, such as prolonged drought, JA signaling initially increases to enhance basal metabolic processes. Once the plants have acclimated to the stress, JA signaling reverts to baseline levels. Chronic stress signals inhibit acute defense pathways, including the rapid synthesis of flavonoids, thereby redirecting carbon flux predominantly towards phenylpropanoid and steroid biosynthesis. Phenylpropanoid biosynthesis generates precursors, such as coumestan coenzyme A, which are essential for flavonoid synthesis and contribute to the extensive distribution of resin within the xylem, culminating in the formation of whole-body resin-containing samples. Concurrently, chronic stress signals activate HMG-CoA reductase within the MVA pathway, channeling acetyl-CoA metabolic flux preferentially towards the synthesis of unsaturated fatty acids. This process leads to the accumulation of γ-linolenic acid, which is crucial for maintaining membrane fluidity and ensuring uniform lipid saturation in xylem cell walls. Saturated fatty acids play a role in the remodeling of cell membrane lipids, thereby preserving the integrity of damaged tissues. They additionally facilitate resin deposition, enhance membrane stability, reduce transpiration, and establish lipid energy reserves, thereby enabling long-term adaptation to drought conditions[57]. Consequently, the morphology of MZ represents a defensive response that involves the repair of membrane systems under moderate, persistent stress and promotes uniform resin deposition within vascular bundles.

The hollow cork cambium sample (P) represents a structural repair mechanism. During the initial phase of damage or in the later stages of acute stress, the reconstruction of physical barriers takes precedence over chemical defense mechanisms. The secondary activation of JA, derived from α-linolenic acid, induces a limited alteration in phenylpropanoid metabolism, promoting the deposition of lignin monomers and suberin to form a cutin/suberin barrier that isolates the damaged area. Concurrently, the flavonoid synthesis pathway is suppressed, resulting in the sacrifice of local tissue to preserve the integrity of the whole organism, and resin synthesis is inhibited[67]. Starch and sucrose metabolism are

significantly activated, leading to their rapid degradation into UDP-glucose and other precursors necessary for cell wall synthesis, thereby providing carbon sources essential for cork layer formation. Consequently, the P form is indicative of mild or older damage, characterized by a reallocation of carbon resources towards regeneration and repair, a reduction in defense signaling, and the substitution of chemical defenses with physical barriers, exhibiting the lowest efficiency in lignification.

3.4.6 Metabolic pathway networks

The fundamental mechanism underlying fat accumulation in Dracaena draconis involves a cascade reaction triggered by tissue damage. Upon damage, reactive ROS activate the LOX pathway, which facilitates the synthesis of JA. Subsequently, JA induces the degradation of JAZ proteins, thereby liberating MYB/bHLH transcription factors. This dual regulatory mechanism enhances phenylpropanoid metabolism by increasing the activity of PAL and CHS, which in turn drives flavonoid biosynthesis. Concurrently, it inhibits the activity of C4H and POD, thereby obstructing the lignin biosynthetic pathway. Ultimately, the flavonoid compounds undergo oxidation and polymerization to form a deep red resin at the wound site, providing a dual barrier of physical sealing and chemical antibacterial activity[58,59].

According to the metabolic pathway network illustrated in Fig. 7D, the phenylpropane pathway emerges as the sole common pathway among the three forms, serving as the central hub that interconnects them. However, the downstream products of this pathway exhibit distinct differentiation. Specifically, LZ is enriched in sinapyl alcohol, which contributes to defense mechanisms via sphingolipids. In contrast, MZ is enriched in sinapate, functioning as an intermediate in the phenylpropanoid pathway. This serves a dual role: as a reserve of flavonoid precursors for LZ defense and as a lignin monomer for P repair, thereby maintaining bidirectional plasticity in downstream pathways. Meanwhile, P is enriched in coniferyl aldehyde, which is utilized for lignin deposition. Although the flavonoid biosynthesis pathway is shared by LZ and P, LZ uniquely accumulates terminal defensive flavonoids, such as pinocembrin and apigenin, through acute JA signaling. This rapid accumulation forms a chemical antibacterial barrier to seal wounds. Conversely, P retains only basic precursors, such as isoliquiritigenin. Carbon sources are preferentially allocated to starch and sucrose metabolism and cell wall repair, with flavonoid synthesis functioning primarily as a supplementary process. Both LZ and P exhibit enrichment in pathways related to starch and sucrose metabolism, as well as galactose metabolism, which collectively supply energy for the synthesis of defensive compounds. As a metabolic intermediate, MZ integrates the structural repair attributes of P with certain defensive capabilities of LZ, while also generating distinctive lipid adaptogens. This leads to a pronounced metabolic divergence, characterized by MZ's defensive polarization, LZ's emphasis on structural repair, and P's repair orientation. Consequently, when directly comparing LZ and P, the differences in these shared pathways become less pronounced, resulting in the identification of fewer significant differences.

In summary, the three resin-containing compounds identified in Dracaena cochinchinensis (P, MZ, and LZ) do not function independently; instead, they constitute a progressive metabolic continuum. This continuum spans from basic repair (P), through lipid adaptation (MZ), to defense activation (LZ), and ultimately cycles back to basic repair (P) in response to late acute stress. This model effectively

illustrates the dynamic strategies of resource allocation and metabolic reprogramming that plants employ in response to varying intensities and types of stress. These strategies range from the activation of chemical defenses and lipid reserve management to basic maintenance. The elucidation of this metabolic continuum provides novel insights into the artificial targeting and induction of Dracaena draconis formation.

4. Conclusion

This study employed UPLC-Q-TOF-MS/MS non-targeted metabolomics in conjunction with FBMN molecular network technology to conduct a comprehensive analysis of the differences in non-volatile metabolites among three resin-containing drugs derived from Dracaena cochinchinensis. A total of 314 compounds were identified, with the majority being flavonoids (81), lipids (65), and phenolic derivatives (50). Multivariate statistical analysis demonstrated a significant distinction between the metabolic profiles of the three samples. The LZ morphology exhibited enrichment in pathways such as linoleic acid metabolism and flavonoid biosynthesis, with high expression levels of defensive flavonoids (e.g., 7-hydroxyflavone), terpenoids (e.g. α-bisabolol), and phenylamines. This morphology promotes the rapid synthesis of flavonoids through heightened JA signaling, resulting in the formation of local resin-secreting aggregated samples. This corresponds to a chemical defense strategy against high-intensity acute stress. Conversely, the MZ morphology was enriched in pathways related to steroid biosynthesis and was characterized by the presence of steroids (e.g. cholesterol), lipids (e.g. γ-linolenic acid), and saponins. This morphological adaptation facilitates chronic drought resilience by maintaining lipid homeostasis and enabling membrane repair, which results in consistent resin deposition. The P form enhances pathways such as starch and sucrose metabolism and α-linolenic acid metabolism, while upregulating lignin monomers (e.g. pinene) and sugars. It prioritizes the allocation of carbon resources towards the repair of physical barriers (e.g. corkification), suppresses resin synthesis, and adapts to mild or chronic damage. This study introduces the progressive metabolic continuum model “P→MZ→LZ→P”for the first time, elucidating how D. cochinchinensis responds to stress gradients through dynamic resource allocation and providing a theoretical foundation for targeted resin induction.

Declarations

Author contributions

Acquisition, analysis, and interpretation of the data: Jiahui Ren and Guang Li; approval of the final manuscript version to be published and confirmation of the authenticity of all raw data: Meijia Chen, Guang Li, Jinhua Su, Jinhui Wang and Yu Zhu. Manuscript drafting: Meijia Chen, Yunfei Cui and Yu Zhu. Critical revisions on the intellectual content: Meijia Chen.

Funding

This study was supported by the Chinese Academy of Medical Sciences (CAMS) Science and Technology Innovation Project for Medicine and Health (2021-I2M-1-031) ,CAMS Innovation Fund for Medical Sciences (CIFMS) ,Yunnan Science and Technology Talent and Platform Program

(202405AF140073) ,Major Science and Technology Special Project of Yunnan Province (202402AA310041)

Data availability

The data generated in the present study are included in the figures and/or tables of this article.

Competing interests

The authors declare no competing interests.

Informed consent

Written informed consent was obtained from all individual participants included in the study.

Footnotes

Publisher's note

Springer Nature remains neutral with regard to jurisdictional claims in published maps and institutional affiliations.

Meijia Chen and Yunfei Cui contributed to equal work.

Contributor Information

Meijia Chen, Email: 18043919006@163.com

Yunfei Cui, Email: cyf719318@163.com

References

1. Zhu, Y. et al. Anti-Helicobacter pylori and Thrombin Inhibitory Components from Chinese Dragon's Blood, Dracaena cochinchinensis. *J. Nat. Prod.* **70**, 1570–1577 (2007).
2. Lang, G. Z. et al. Bioactive flavonoid dimers from Chinese dragon's blood, the red resin of *Dracaena cochinchinensis*. *Bioorg. Chem.* **97**, 103659 (2020).
3. Xu, L., Zhou, Z., Chen, Y., Lu, H. & Hu, P. Resina Draconis Particles Encapsulated in a Hyaluronic-Acid-Based Hydrogel to Treat Complex Burn Wounds. *Pharmaceutics* **14**, 2087 (2022).
4. Zhang, L., Ke, W., Zhao, X. & Lu, Z. Resina Draconis extract exerts anti-HCC effects through METTL3-m6A-Survivin axis. *Phytother Res.* **36**, 2542–2557 (2022).
5. Wen, F., Zhao, X., Zhao, Y., Lu, Z. & Guo, Q. The anticancer effects of Resina Draconis extract on cholangiocarcinoma. *Tumor Biol.* **37**, 15203–15210 (2016).
6. Xin, N. et al. Dragon's Blood extract has antithrombotic properties, affecting platelet aggregation functions and anticoagulation activities. *J. Ethnopharmacol.* **135**, 510–514 (2011).

7. Wang, X. H., Zhang, C., Yang, L. L. & Gomes-Laranjo, J. Production of dragon's blood in *dracaena cochinchinensis* plants by inoculation of *fusarium proliferatum*. *Plant. Sci.* **180**, 292–299 (2011).
8. Su et al. Comparative study on differences of resin-containing drugs in Dracaena from different appearance based on HS-GC-MS and chemometrics. *China J. Chin. Materia Med.* **45**, 3467–3474 (2020).
9. Patel, M. K. et al. Plants Metabolome Study: Emerging Tools and Techniques. *Plants* **10**, 2409 (2021).
10. Delfin, J. C., Watanabe, M. & Tohge, T. Understanding the function and regulation of plant secondary metabolism through metabolomics approaches. *Theor. Exp. Plant. Physiol.* **31**, 127–138 (2019).
11. Ma, A. & Qi, X. Mining plant metabolomes: Methods, applications, and perspectives. *Plant. Commun.* **2**, 100238 (2021).
12. Nothias, L. F. et al. Feature-based molecular networking in the GNPS analysis environment. *Nat. Methods*. **17**, 905–908 (2020).
13. Li, Y. et al. Identifying distinct markers in two sorghum varieties for baijiu fermentation using untargeted metabolomics and molecular network approaches. *Food Chem. X*. **23**, 101646 (2024).
14. Li, W. et al. Metabolite fingerprinting of the ripening process in pixian douban using a feature-based molecular network and metabolomics analysis. *Food Chem.* **418**, 135940 (2023).
15. Kim, H. W. et al. NPClassifier: a deep neural network-based structural classification tool for natural products. *J. Nat. Prod.* **84**, 2795–2807 (2021).
16. Wojtanowski, K. K. & Mroczek, T. Detection, identification and structural elucidation of flavonoids using liquid chromatography coupled to mass spectrometry. *Curr Org. Chem* **24**, 104–112 .
17. Jiang, C. & Gates, P. J. Systematic characterisation of the fragmentation of flavonoids using high-resolution accurate mass electrospray tandem mass spectrometry. *Molecules* **29**, 5246 (2024).
18. March, R. & Brodbelt, J. Analysis of flavonoids: tandem mass spectrometry, computational methods, and NMR. *J. Mass. Spectrom.* **43**, 1581–1617 (2008).
19. Sun, Q. et al. Chemical constituents of crinum asiaticum L. var. sinicum baker and their cytotoxic activities. *Chem. Biodivers.* **6**, 1751–1757 (2009).
20. Khalifa, M. F. et al. Studies on the nonalkaloidal secondary metabolites of hippeastrum vittatum (L'her.) herb. Bulbs. *ACS Omega*. **8**, 26749–26761 (2023).
21. Soliman, M. S. M. et al. Pharmacological activities and characterization of phenolic and flavonoid compounds in methanolic extract of euphorbia cuneata vahl aerial parts. *Molecules* **26**, 7345 (2021).
22. Xie, J., Zhang, Y., Wang, W. & Hou, J. Identification and simultaneous determination of glycyrrhizin, formononetin, glycyrrhetinic acid, liquiritin, isoliquiritigenin, and licochalcone a in licorice by LC-MS/MS. *Acta Chromatographica*. **26**, 507–516 (2014).
23. Xue, F. et al. Simultaneous determination of 14 bioactive components in fangji huangqi tang by UHPLC-QqQ-MS technique. *Biomed. Chromatogr.* **39**, e70073 (2025).

24. Qu, T. et al. Network pharmacology, molecular docking, molecular dynamics simulation, and experiment verification analysis to reveal the action mechanism of RenShen guipi wan in the treatment of anemia. *Biotechnol. Lett.* **47**, 1–13 (2025).
25. Ga, S. & A, N. Bioflavonoids ameliorate crowding induced hemoglobin aggregation: a spectroscopic and molecular docking approach. *Pubmed* (2025).
26. Sangweni, N. F. et al. Doxorubicin-induced cardiomyopathy: a preliminary study on the cardioprotective benefits of 7-hydroxyflavanone. *Int. J. Mol. Sci.* **24**, 15395 (2023).
27. Sengupta, B., Sahihi, M., Dehkhodaei, M., Kelly, D. & Arany, I. Differential roles of 3-hydroxyflavone and 7-hydroxyflavone against nicotine-induced oxidative stress in rat renal proximal tubule cells. *PLOS One*. **12**, e0179777 (2017).
28. Qi, X. et al. 7-hydroxyflavone improves nonalcoholic fatty liver disease by acting on STK24. *Phytother Res.* **38**, 3444–3458 (2024).
29. Wan, L. Q., Tan, Y., Jiang, M. & Hua, Q. The prognostic impact of traditional chinese medicine monomers on tumor-associated macrophages in non-small cell lung cancer. *Chin. J. Nat. Med.* **17**, 729–737 (2019).
30. Calderone, V. et al. Vasorelaxing effects of flavonoids: investigation on the possible involvement of potassium channels. *Naunyn Schmiedebergs Arch. Pharmacol.* **370**, 290–298 (2004).
31. Shi, D. et al. The antioxidant activity and neuroprotective mechanism of isoliquiritigenin. *Free Radic Biol. Med.* **152**, 207–215 (2020).
32. Soromou, L. W. et al. Regulation of inflammatory cytokines in lipopolysaccharide-stimulated RAW 264.7 murine macrophage by 7-O-methyl-naringenin. *Molecules* **17**, 3574–3585 (2012).
33. Ahmed, M. S. et al. A weakly antimalarial biflavanone from *rhus retinorrhoea*. *Phytochemistry* **58**, 599–602 (2001).
34. Takahashi, L. K. et al. Vacuum-ultraviolet photoionization and mass spectrometric characterization of lignin monomers coniferyl and sinapyl alcohols. *J. Phys. Chem. A.* **115**, 3279–3290 (2011).
35. Yamaguchi, A., Kishimoto, T. & Urabe, D. Initial stage of syringyl lignin formation from sinapyl alcohol. *J. Agric. Food Chem.* **71**, 14666–14677 (2023).
36. Zhang, Y. et al. Lr34/Yr18/Sr57/Pm38 confers broad-spectrum resistance to fungal diseases via sinapyl alcohol transport for cell wall lignification in wheat. *Plant. Commun.* **5**, 12, 9 (2024).
37. Choi, J. et al. Anti-inflammatory and antinociceptive effects of sinapyl alcohol and its glucoside syringin. *Planta Med.* **70**, 1027–1032 (2004).
38. Perbellini, L. et al. Determination of alpha-bisabolol in human blood by micro-HPLC–ion trap MS and head space-GC–MS methods. *J. Chromatogr. B.* **812**, 373–377 (2004).
39. Wu, Y. et al. Exploring the mechanism of α-bisabolol in the treatment of psoriasis based on network pharmacology and experimental validation. *Eur. J. Pharmacol.* **999**, 177433 (2025).
40. Vm, M. P., Mi, O., Ha, P. M. & G, B. R. V, M.-P. Anti-inflammatory and utero-relaxant effect of α-bisabolol on the pregnant human uterus. *Pubmed* (2025).

41. Barreto, R. S. S. et al. Evidence for the involvement of TNF-α and IL-1β in the antinociceptive and anti-inflammatory activity of *stachys lavandulifolia* vahl. (lamiaceae) essential oil and (-)-α-bisabolol, its main compound, in mice. *J. Ethnopharmacol.* **191**, 9–18 (2016).
42. Eddin, L. B. et al. Health benefits, pharmacological effects, molecular mechanisms, and therapeutic potential of α-bisabolol. *Nutrients* **14**, 1370 (2022).
43. Shi, D. et al. The antioxidant activity and neuroprotective mechanism of isoliquiritigenin. *Free Radic Biol. Med.* **152**, 207–215 (2020).
44. Ali, F. & Rahul Naz,Falaq, Jyoti, Smita & and Siddique, Y. H. Health functionality of apigenin: a review. *Int. J. Food Prop.* 20, 1197–1238 (2017).
45. Pearce, G., Marchand, P. A., Griswold, J., Lewis, N. G. & Ryan, C. A. Accumulation of feruloyltyramine and *p*-coumaroyltyramine in tomato leaves in response to wounding. *Phytochemistry* **47**, 659–664 (1998).
46. Negrel, J., Pollet, B. & Lapierre, C. Ether-linked ferulic acid amides in natural and wound periderms of potato tuber. *Phytochemistry* **43**, 1195–1199 (1996).
47. Zhao, Q. Lignification: flexibility, biosynthesis and regulation. *Trends Plant. Sci.* **21**, 713–721 (2016).
48. Yoshioka, K. et al. Hydroxycinnamaldehyde-derived benzofuran components in lignins. *Plant. Physiol.* **194**, 1370–1382 (2024).
49. Yamamoto, M., Blaschek, L., Subbotina, E., Kajita, S. & Pesquet, E. Importance of lignin coniferaldehyde residues for plant properties and sustainable uses. *ChemSusChem* **13**, 4400–4408 (2020).
50. He, M. & Ding, N. Z. Plant unsaturated fatty acids: multiple roles in stress response. *Front Plant. Sci* **11**, (2020).
51. Zhu, Y. et al. GhPLP2 positively regulates cotton resistance to verticillium wilt by modulating fatty acid accumulation and jasmonic acid signaling pathway. *Front Plant. Sci* **12**, (2021).
52. Ma, Q. et al. Exogenous methyl jasmonate induces *CHS* and promotes flavonoid accumulation in *zanthoxylum bungeanum*. *Ind. Crops Prod.* **222**, 119682 (2024).
53. Liu, Z. et al. Uncovering the role of hydroxycinnamoyl transferase in boosting chlorogenic acid accumulation in carthamus tinctorius cells under methyl jasmonate elicitation. *Int. J. Mol. Sci.* **25**, 2710 (2024).
54. Y, C. et al. The jasmonate-induced bHLH gene SlJIG functions in terpene biosynthesis and resistance to insects and fungus. *Pubmed* (2025).
55. Kamali, S., Iranbakhsh, A., Ebadi, M., Oraghi Ardebili, Z. & Haghighat, S. Methyl jasmonate conferred arsenic tolerance in *thymus kotschyanus* by DNA hypomethylation, stimulating terpenoid metabolism, and upregulating two cytochrome P450 monooxygenases. *J. Hazard. Mater.* **465**, 133163 (2024).
56. Liu, Z. et al. Regulation, evolution, and functionality of flavonoids in cereal crops. *Biotechnol. Lett.* **35**, 1765–1780 (2013).

57. Sonawane, P. D. et al. Plant cholesterol biosynthetic pathway overlaps with phytosterol metabolism. *Nat. Plants*. **3**, 16205 (2016).

58. Jura-Morawiec, J. & Tulik, M. Dragon's blood secretion and its ecological significance. *Chemoecology* **26**, 101–105 (2016).

59. Xu, Y. et al. A chromosome-level genome assembly for *dracaena cochinchinensis* reveals the molecular basis of its longevity and formation of dragon's blood. *Plant. Commun.* **3**, 100456 (2022).

Figures

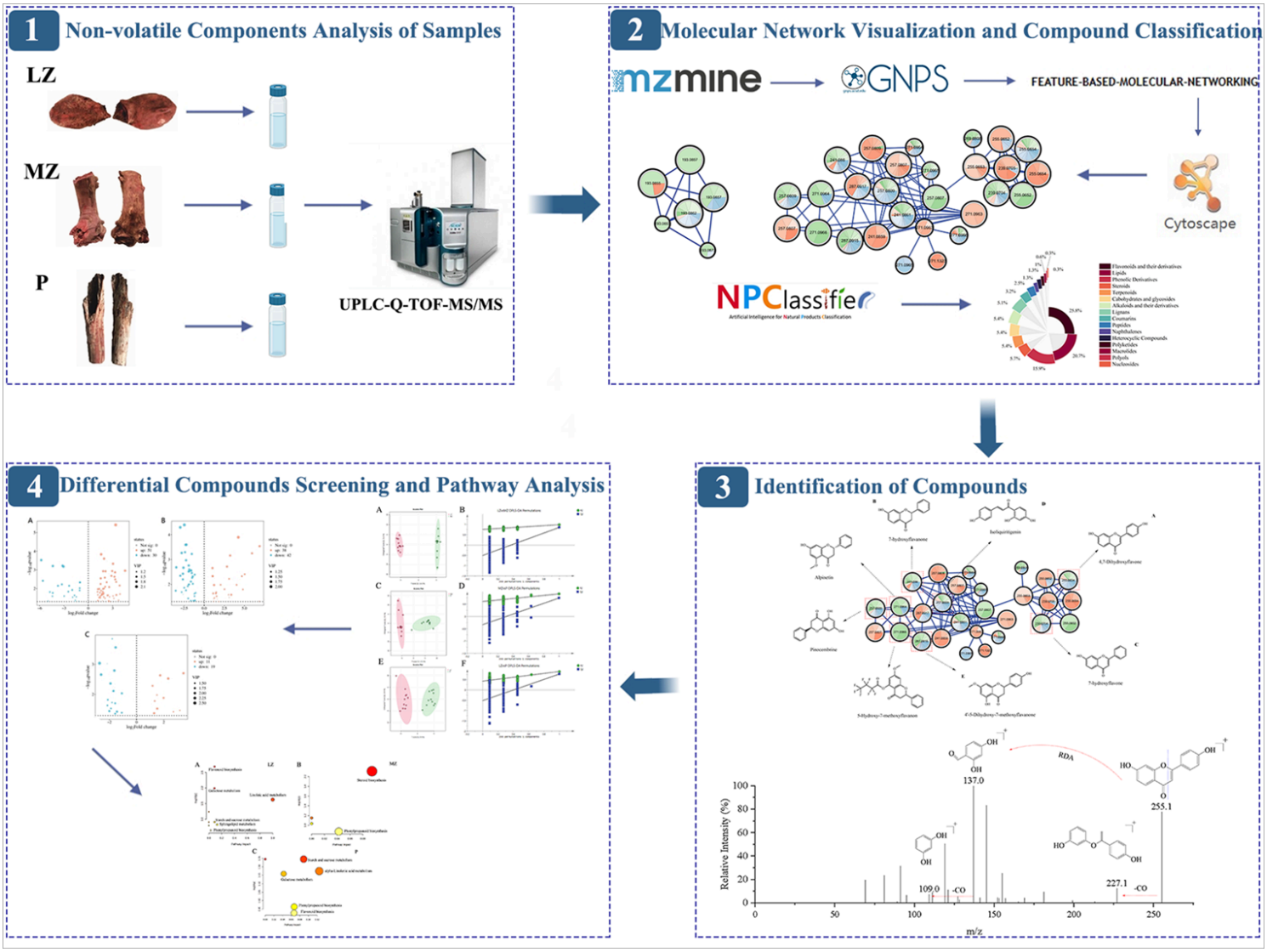

Figure 1

Schematic representation of the workflow of the study

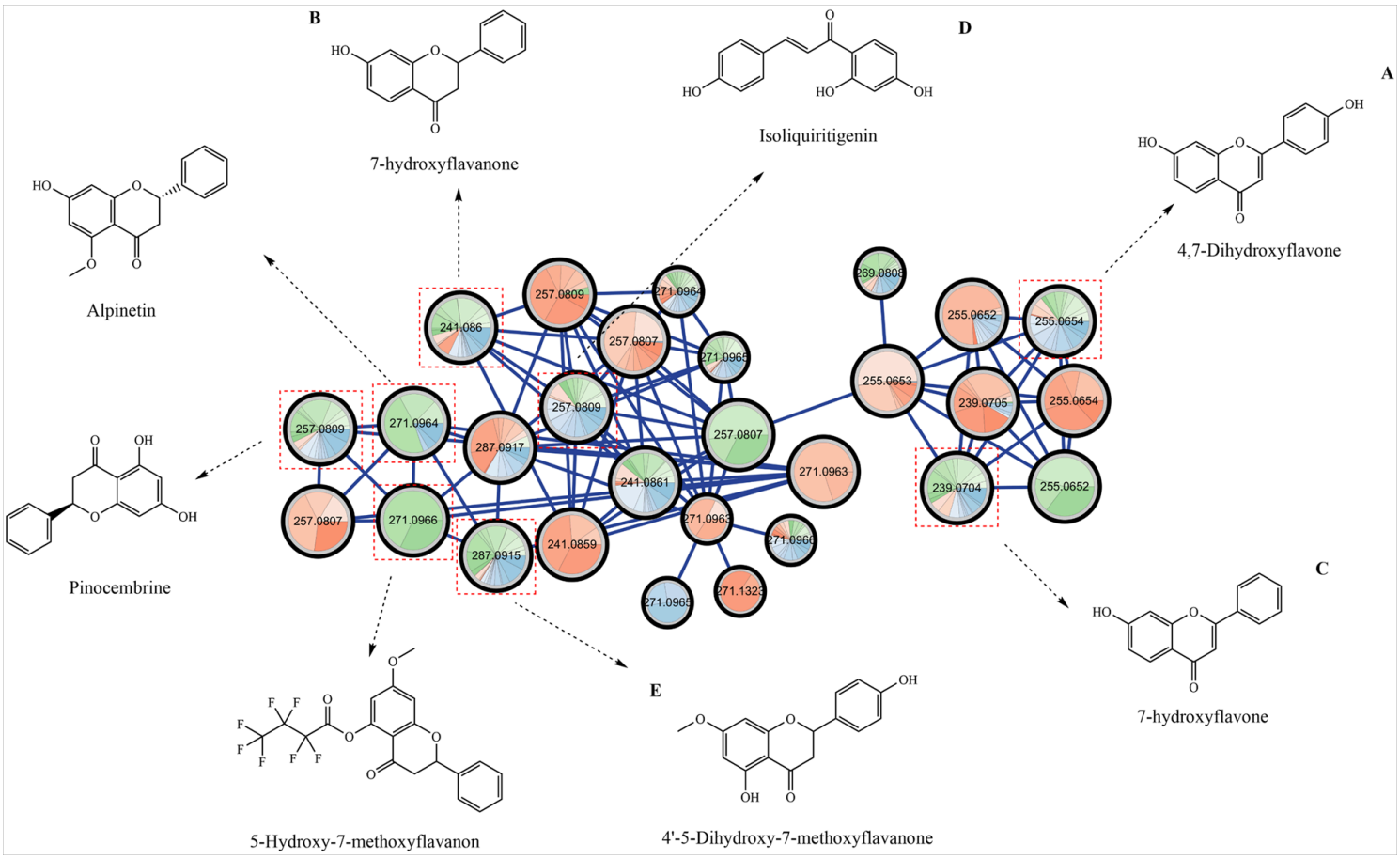

Figure 2

Flavonoid compound molecular family

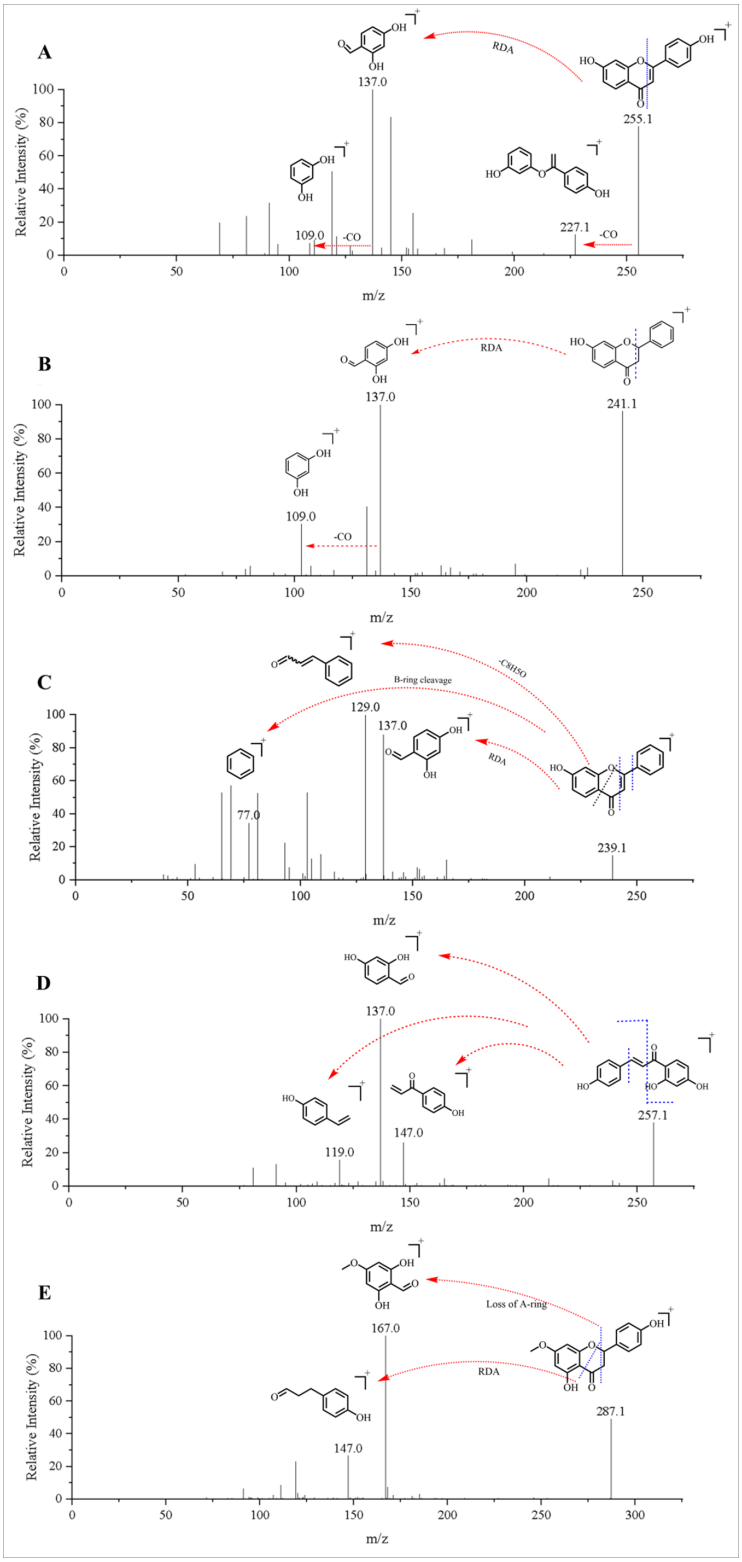

Figure 3

Structural annotations of key flavonoid compounds

A□4,7-Dihydroxyflavone□B□7-Hydroxyflavanone□C□7-Hydroxyflavone□D□Isoliquiritigenin□E□4'-5-Dihydroxy-7-methoxyflavanone

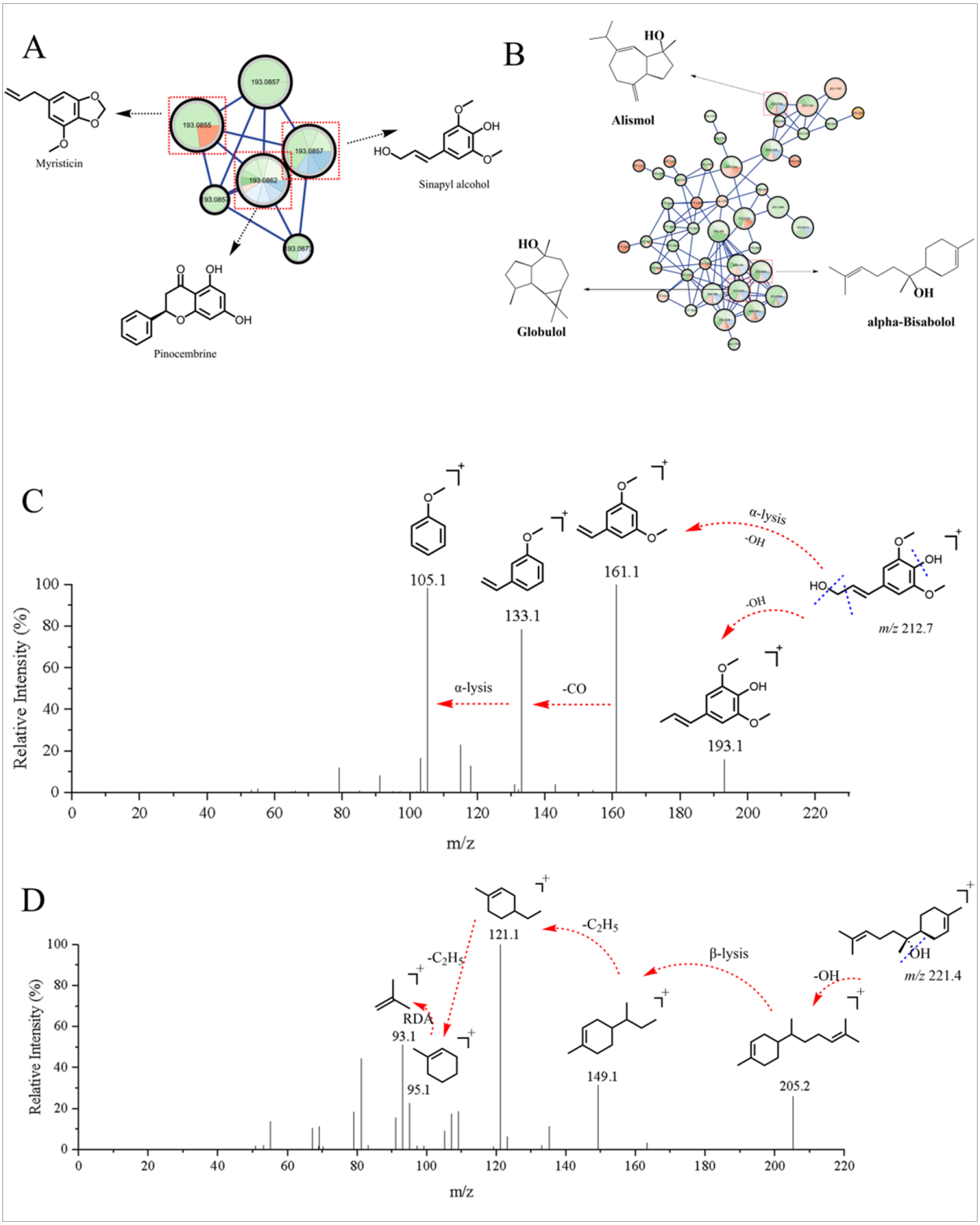

Figure 4

Phenolic and Terpenoid Molecular Families and Structural annotations of key compounds

A: Phenolic Compound Molecular Families; B: Terpenoid Molecular Families; C:Structural annotation of Sinapyl alcohol; D:Structural annotation of α-Bisabolol

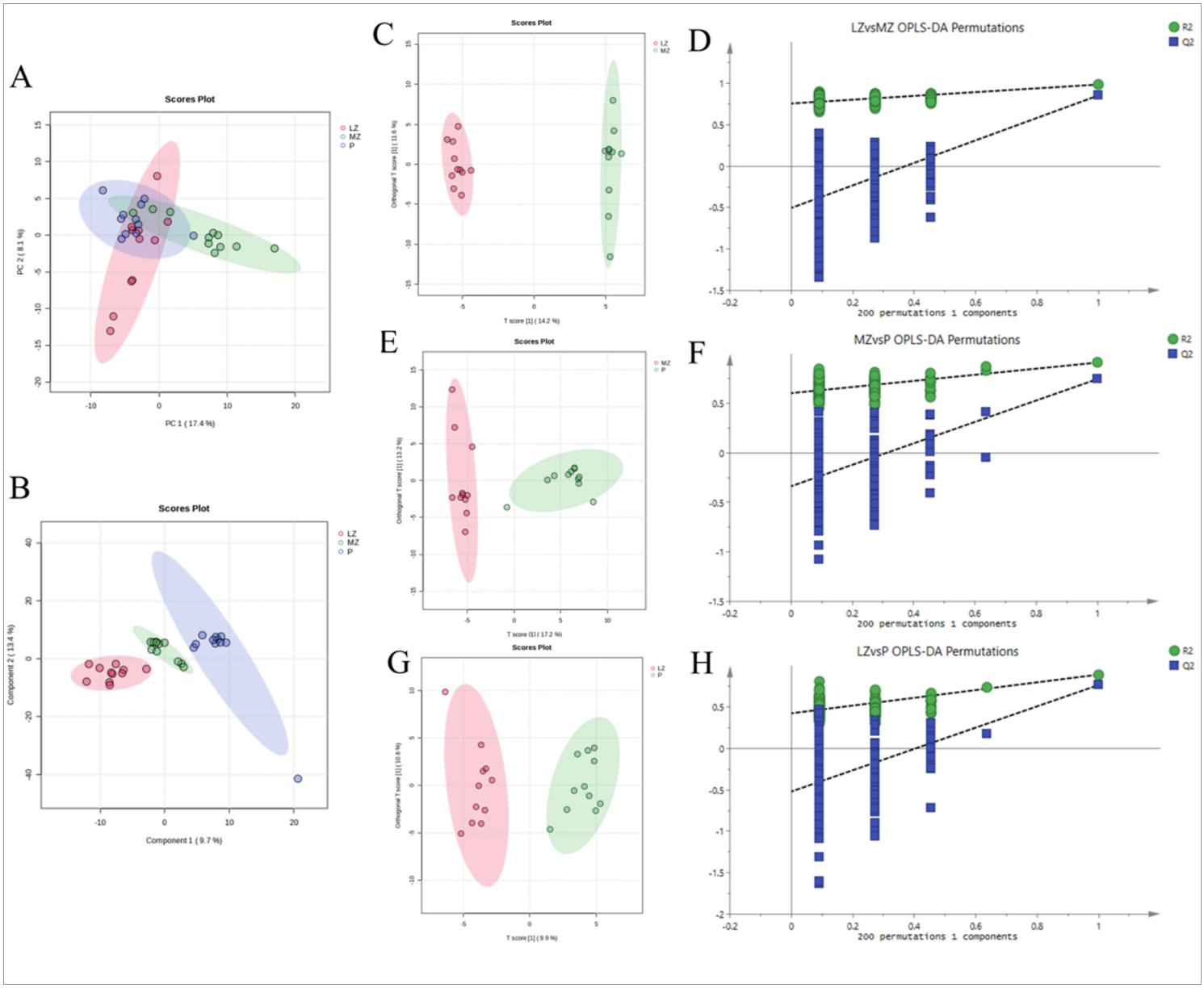

Figure 5

PCA, PLS-DA and OPLS-DA analyses of resin-containing herbs of different forms of dragon blood trees

A:PCA analysis of Different forms of dragon blood trees resin-containing herbs; B:PLSDA analysis of Different forms of dragon blood trees containing herbs; C, E, and G are two-by-two group comparisons of OPLS-DA

D, F, and I are two-by-two group comparisons of OPLS-DA model replacement test plots

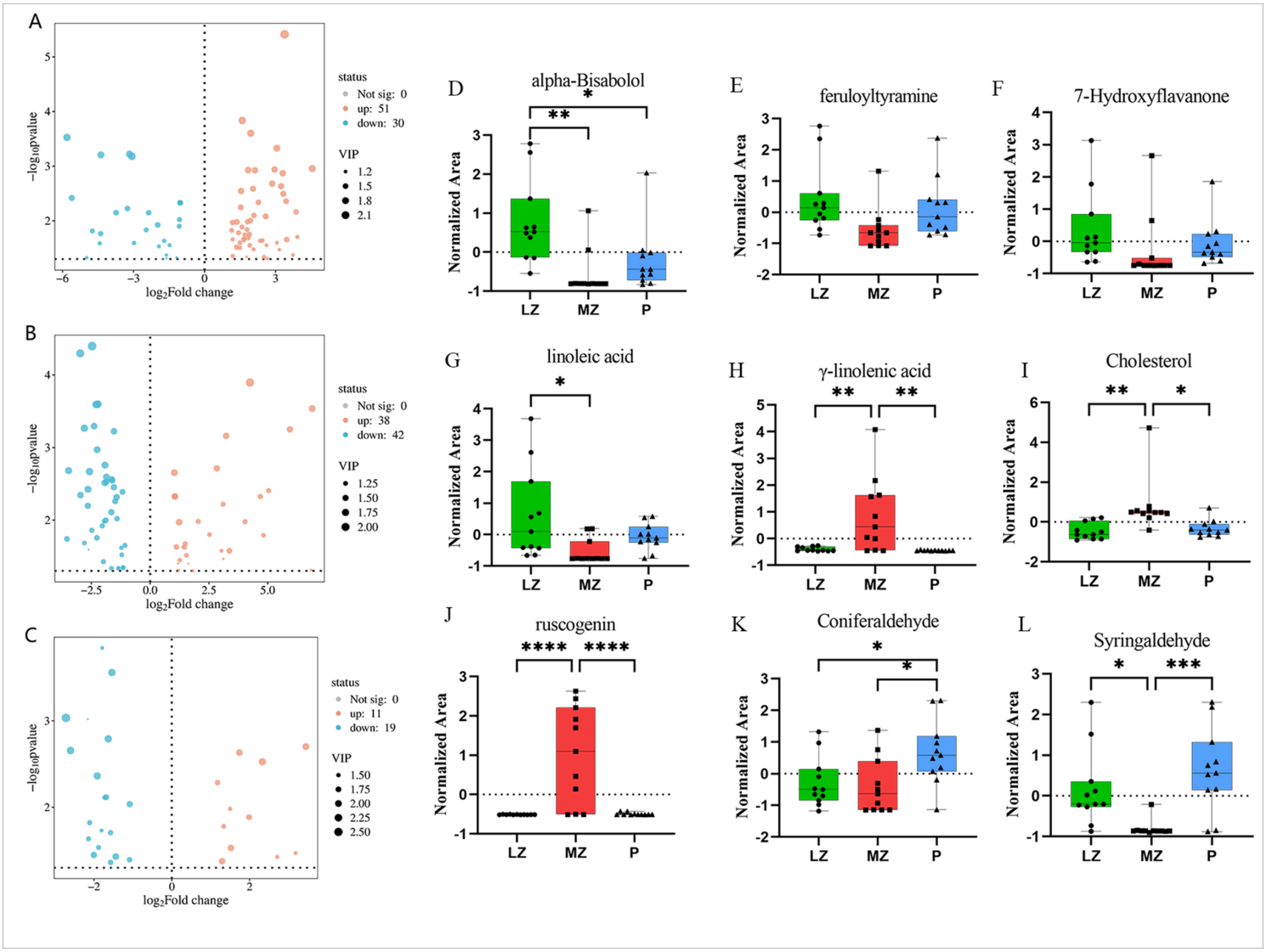

Figure 6

Volcano plots for two-by-two comparisons and box plots for nine differential compounds

A-C is Volcano plots comparing the three forms of dragon's blood and their differentiated compounds in pairs; D-E are box plots, D：alpha-Bisabolol；E：feruloyltyramine；F：7-Hydroxyflavanone；G：linoleic acid；H：γ-linolenic acid；I：Cholesterol；J：ruscogenin；K：Coniferaldehyde；L：Syringaldehyde

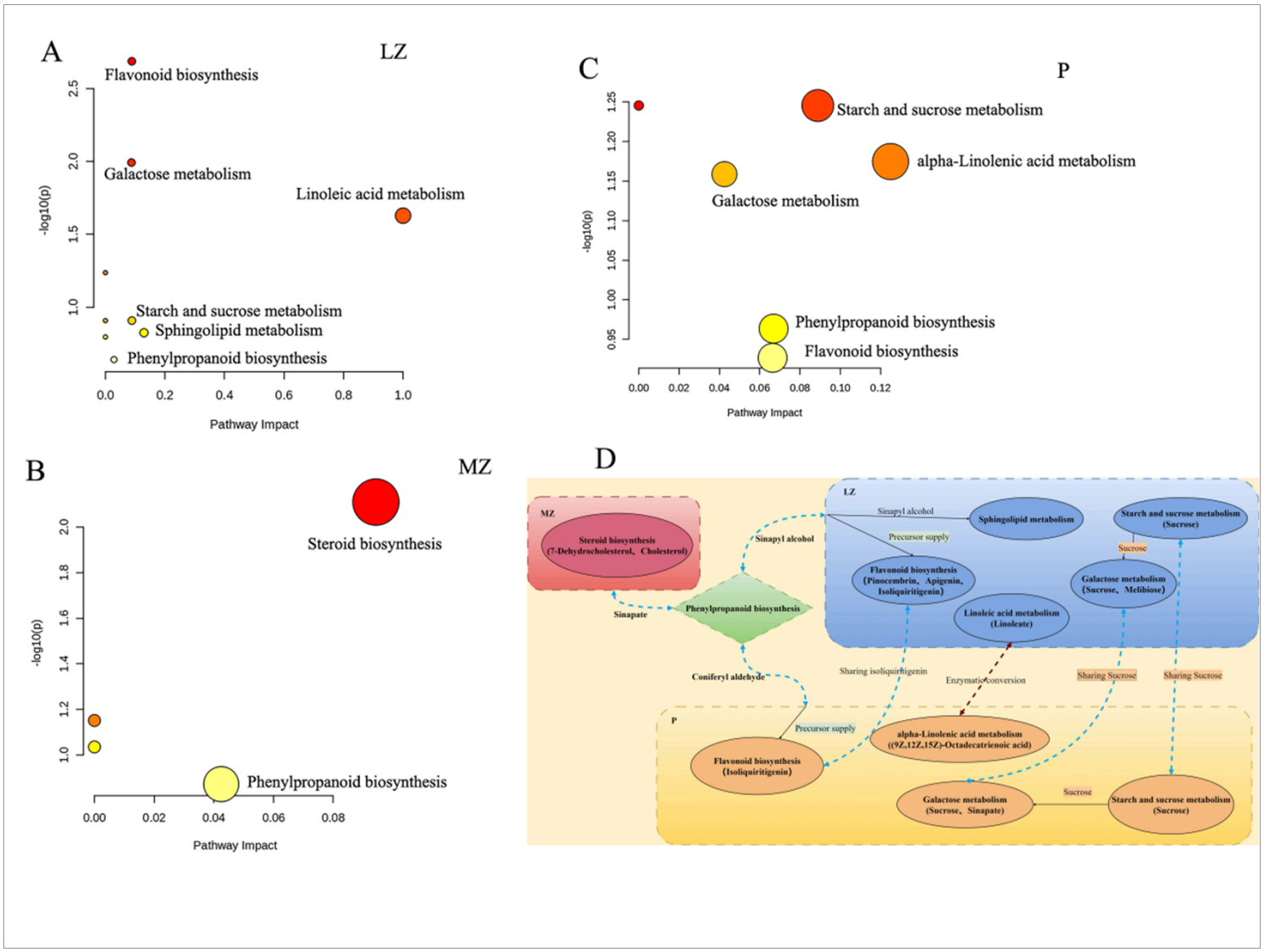

Figure 7

Pathway enrichment diagram of the first 25 differential compounds of the three forms of Dracaena Draconis and Metabolic pathway network diagram of the three forms of Dracaena Draconis

Supplementary Files

This is a list of supplementary files associated with this preprint. Click to download.

- SupplementaryMaterial.docx